Local mode analysis of characteristic vibrational coupling in nucleobases and Watson–Crick base pairs of DNA

IOP Publishing Electron. Struct. 4 (2022) 044005 https://doi.org/10.1088/2516-1075/acaa7a

Electronic Structure

PAPER

Local mode analysis of characteristic vibrational coupling in nucleobases and Watson–Crick base pairs of DNA

Mateus Quintano[1], **Alexis A A Delgado**[1], **Renaldo T Moura Jr**[1,2], **Marek Freindorf**[1] **and Elfi Kraka**[1,*]

[1] Computational and Theoretical Chemistry Group (CATCO), Department of Chemistry, Southern Methodist University, Dallas, TX 75275, United States of America
[2] Department of Chemistry and Physics, Center of Agrarian Sciences, Federal University of Paraiba, Areia, PB, Brazil
[*] Author to whom any correspondence should be addressed.

E-mail: ekraka@gmail.com

RECEIVED
29 September 2022

REVISED
30 October 2022

ACCEPTED FOR PUBLICATION
9 December 2022

PUBLISHED
28 December 2022

Keywords: local vibrational mode analysis, characterization of normal mode procedure, DNA, base pairs, vibrational base pair coupling

Abstract

Two-dimensional infrared spectroscopy has reported highly delocalized in-plane base vibrations in the fingerprint region of nucleotide monophosphates, suggesting the involvement of base pair C=O and C=C ring bonds and considerable interaction between C=O bond stretches. The high delocalization results in congested vibrational spectra, which complicates the assignment of the peaks. This congestion also extends to Watson–Crick base pairs. We applied in this work the characterization of normal mode procedure, a special feature of our local mode analysis, and could for the first time identify the C=O and C=C bonds being engaged in base pair coupling and quantify their contribution to each of the delocalized fingerprint vibration. In addition, a detailed and quantitative description of the hydrogen bonds involved in the Watson–Crick base pairs was provided. Based on the results of this study, we developed a new protocol to elucidate on the assignment of bands in the vibrational spectra of nucleic acids by probing the vibrational space for specific interactions between functional groups prior to and upon base pairing. This protocol will aid to fill the gap between deoxyribonucleic acid structural information and vibrational spectroscopy experiments by facilitating the interpretation of spectra on a quantitative basis.

1. Introduction

Deoxyribonucleic acid (DNA) is a nucleotide-made polymer of genetic, catalytic and structural importance, whose double-stranded nature is governed by complementary base pairing through specific hydrogen bonds [1]. As illustrated in figure 1, the resulting Watson–Crick structure is comprised of two types of base pairs, that is, adenine (A) and guanine (G) must pair with thymine (T) and cytosine (C), respectively [1, 2]. Information on the structure of nucleic acids and their interactions are of particular interest to linear and nonlinear vibrational spectroscopy investigations [3–20]. Within the frequency range of 1500−1800 cm^{-1} are the in-plane base vibrations (fingerprint or characteristic region).

In computational investigations in-plane base vibrations are usually restricted to the nucleobases with the methyl group as a cost-effective replacement for the phosphate and sugar groups [6, 7]. These simulations usually take into account hydration effects and deuterium in place of labile amino hydrogen atoms to provide a more realistic quantum chemical approach to vibrational spectra [3, 6, 7, 10, 14]. Deuterium effects are accounted for as experimental measurements are usually performed in deuterated water to circumvent interference of the HOH bending mode [19]. Deuterium effects dramatically change the fingerprint region of the spectra by shifting ND and ND_2 scissoring and stretching mode frequencies to regions outside the characteristic one [3, 7]. Hence, in the realm of deuteration effects, the focus is on C=O stretching and ring deformation modes [7].

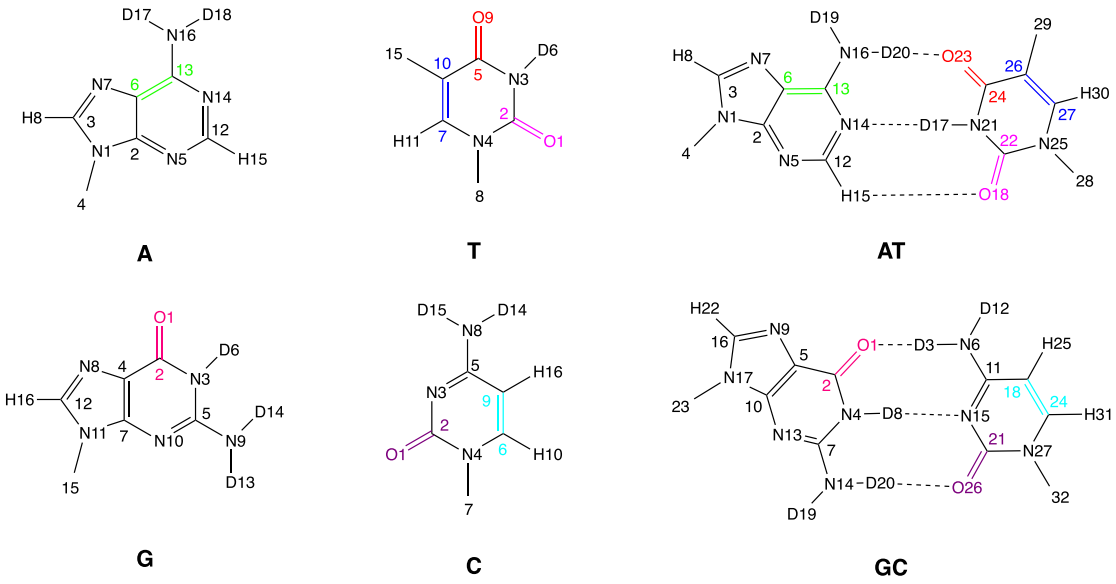

Figure 1. Suggested C=O and C=C bonds (in color) of methylated nucleobases A, G, T, and C models being involved in base pair coupling [10, 18, 19]. Index numbers refer to the numbering of atoms used in this work. Terminal carbon atoms of the methyl groups are indicated by numbers without atomic symbols.

The sensitivity of IR spectroscopy to changes in the secondary structure of DNA can be linked to specific normal vibrational modes in the fingerprint region [3–7, 15–20]. In this respect, the search for a theoretical framework that contributes to the elucidation of the couplings (interactions) involving C=O and C=C vibrations has been of recent interest [10, 18, 19]. It has been suggested that particular nucleobase C=C and C=O bonds engage in base pair couplings, as highlighted in figure 1

However, the high delocalization of normal vibrational modes has made it hard to pinpoint bond stretching contributions even for the building blocks of nucleic acids, as revealed by 2D IR measurements of the in-plane base vibrations of nucleotide monophosphates [10]. Normal vibrational modes usually tend to extend over aromatic rings, contain interaction between C=O stretches, and exhibit interdependence between the C=O and C=C groups in the pyrimidine bases [10]. Hydrogen bonding in Watson–Crick base pairs has been reported to influence delocalization and coupling of the fingerprint normal vibrational modes as well [4, 6–9]. Clearly, all of this has called for new ideas to facilitate the interpretation of the vibrational spectra of nucleic acids, which we have materialized in this work via the local mode analysis (LMA), originally proposed by Konkoli and Cremer [21–26] using the characterization of normal mode (CNM) procedure [23, 25] as a key tool.

2. Method

2.1. The Wilson GF formalism

The normal mode analysis machinery describing a vibrating molecule with N atoms is based on the Wilson equation of vibrational spectroscopy [27–31]

$$\mathbf{F}^{x}\mathbf{L} = \mathbf{M}\mathbf{L}\mathbf{\Lambda} \tag{1}$$

where $\mathbf{F}^{x}$ is the $3N \times 3N$ force constant matrix (Hessian matrix) in Cartesian coordinates x_i ($\mathrm{i} = 1, \cdots 3N$). The diagonal $3N \times 3N$ mass matrix $\mathbf{M}$ contains the atomic mass for each atom three times to account for the motion in x, y and z directions. The diagonal matrix $\mathbf{\Lambda}$ contains the eigenvalues λ_μ ($\mu = 1, \cdots, N_{\mathrm{vib}}$; $N_{\mathrm{vib}} = 3N - \Sigma$, $\Sigma = 5$ or 6 for linear and non-linear molecules, respectively), whose relationship with the normal vibrational mode frequencies ω_μ is given by $\lambda_\mu = 4\pi^2 c^2 \omega_\mu^2$, with c being the speed of light. The $3N \times N_{\mathrm{vib}}$ matrix $\mathbf{L}$ collects the normal modes $\mathbf{l}_\mu$ as orthonormal column vectors.

One can also express the molecular geometry in terms of internal coordinates $\mathbf{q}$ rather than Cartesian coordinates $\mathbf{x}$, and by this the Wilson equation adopts a new form [27]:

$$\mathbf{F}^{q}\mathbf{D} = \mathbf{G}^{-1}\mathbf{D}\mathbf{\Lambda} \tag{2}$$

where **D** collects the normal mode vectors $\mathbf{d}_\mu$ ($\mu = 1, \ldots, N_{\text{vib}}$) column-wise, and the Wilson matrix G, which is defined as

$$\mathbf{G} = \mathbf{B}\mathbf{M}^{-1}\mathbf{B}^{\mathrm{T}} \tag{3}$$

whose inverse represents the kinetic energy in terms of internal coordinates. The elements of the rectangular **B** matrix in equation (3) are defined by the partial derivatives of internal coordinates q_n ($n = 1, 2, 3 \ldots N_{\text{vib}}$) with regard to Cartesian coordinates x_i ($i = 1, 2, 3 \ldots 3N$),

$$\mathbf{B}_n = \frac{\delta q_n(x)}{\delta x_i}. \tag{4}$$

It is important to note that the **B** matrix plays a central role for the Wilson equation of spectroscopy, namely connecting different sets of coordinates (internal, symmetry, curvilinear, etc) [32–34] or Cremer-Pople ring puckering coordinates [35], with the Cartesian coordinates [27]. Therefore, whenever a new set of coordinates is introduced, the first step is to derive the appropriate **B** matrix, as demonstrated below for the definition of intermonomer modes.

Diagonalization of equation (2) leads to a transformation to normal coordinates **Q** and the diagonal force constant matrix **K** expressed in normal coordinates (i.e. $\mathbf{K} = \mathbf{K}^{\mathbf{Q}}$) which both play a central role in the normal mode analysis [27]

$$\mathbf{D}^{\mathrm{T}}\mathbf{F}^{q}\mathbf{D} = \mathbf{K}. \tag{5}$$

The transformation to normal coordinates **Q** leading to the diagonal force constant matrix **K** and normal mode vectors $\mathbf{d}_\mu$ (see equation (5)) is a standard procedure in modern quantum chemistry packages calculating vibrational frequencies, providing access to important electronic structure information of a molecule and the motion of its atoms for each of the N_{vib} vibrations [36–38]. Therefore, vibrational frequencies and related force constants have become a popular measure of bond strength.

However, caveat is appropriate. As already pointed out by Wilson in 1941 [39], normal coordinates **Q** are generally a linear combination of internal coordinates **q** or Cartesian coordinates **x**

$$\begin{aligned} \mathbf{Q} &= \tilde{\mathbf{D}}^{\mathrm{T}}\mathbf{G}^{-1}\mathbf{q} \\ &= \tilde{\mathbf{D}}^{\mathrm{T}}\mathbf{G}^{-1}\mathbf{B}\mathbf{x} \end{aligned} \tag{6}$$

where the tilde symbol denotes mass-weighting and $\tilde{\mathbf{D}}$ is renormalized via $\mathbf{D} = \tilde{\mathbf{D}}(\mathbf{L}^{\mathrm{T}}\mathbf{M}\mathbf{L})^{1/2}$. As an important consequence, normal vibrational modes are generally delocalized over the molecule (as e.g. experienced in base pair coupling), limiting the direct use of normal mode frequencies and normal mode force constants as bond strength measure. For this purpose, local vibrational modes and related local mode frequencies and force constants are needed.

2.2. The local vibrational mode theory

The local vibrational mode theory, whose foundations were laid by Konkoli and Cremer [21–25], offers a solution to the delocalization problem. As shown by Konkoli and Cremer, local mode vectors a_n associated with the internal coordinates q_n, can be derived from the normal vibrational modes d_n and the normal mode force constant matrix **K**

$$\mathbf{a}_n = \frac{\mathbf{K}^{-1}\mathbf{d}_n^{\mathrm{T}}}{\mathbf{d}_n\mathbf{K}^{-1}\mathbf{d}_n^{\mathrm{T}}} \tag{7}$$

where it should again be highlighted that d_n and K can be readily obtained from standard quantum chemistry packages after a vibrational frequency calculation.

The local mode force constant k_n^a reads

$$\begin{aligned} k_n^a &= \mathbf{a}_n^{\mathrm{T}}\mathbf{K}\mathbf{a}_n \\ &= \left(\mathbf{d}_n\mathbf{K}^{-1}\mathbf{d}_n^{\mathrm{T}}\right)^{-1} \end{aligned} \tag{8}$$

from which the local mode frequency ω_n^a can be calculated

$$(\omega_n^a)^2 = \left(4\pi^2 c^2\right)^{-1} \frac{k_n^a}{m_n^a}. \tag{9}$$

The local mode mass m_n^a is given by $m_n^a = \left(\mathbf{B}_n\mathbf{M}^{-1}\mathbf{B}_n^{\mathrm{T}}\right)^{-1}$.

In the context of vibrational spectra interpretation, the CNM procedure, an integral part of LMA, offers the possibility of decomposing every normal vibrational mode $\mathbf{l}_\mu$ (associated with absorption peaks) into local vibrational mode percentage contributions from a non-redundant set of N_{vib} local vibrational modes $\mathbf{a_n}$. In this respect, it is necessary to incorporate the overlapping encoded by $S_{n\mu}$ [23–26] (in the discrete scalar product space),

$$S_{n\mu} = \frac{\langle \mathbf{a}_n^x | \mathbf{F}^x | \mathbf{l}_\mu \rangle^2}{\langle \mathbf{a}_n^x | \mathbf{F}^x | \mathbf{a}_n^x \rangle \langle \mathbf{l}_\mu | \mathbf{F}^x | \mathbf{l}_\mu \rangle}. \tag{10}$$

The percentage contribution $C_{n\mu}{}^{\%}$ (local mode character) of local vibrational mode $\mathbf{a}_n$ to normal vibrational mode $\mathbf{l}_\mu$ reads [23]

$$C_{n\mu}^{\%} = \frac{S_{n\mu}}{\sum_m^{N_{\text{vib}}} S_{m\mu}} 100. \tag{11}$$

Recently, CNM has been successfully applied in the investigation of pK_a probes [40] and to gain insights into *vibrational Stark effect* probes [41].

2.3. Analysis of bond strength and bond nature

Zou and Cremer [42] provided the important proof that the local stretching force constant k_n^a(AB) reflects the intrinsic strength of the bond/interaction between two atoms A and B being described by an internal coordinate q_n, qualifying k_n^a(AB) as perfectly suited strength descriptor. It is convenient to base the discussion for larger sets of molecules on a relative bond strength order (BSO) n rather than on a direct comparison of local force constant values. Both are connected via a power relationship of the form

$$\text{BSO } n = A(k^a)^B \tag{12}$$

according to the generalized Badger rule derived by Cremer, Kraka and co-workers [43, 44]. The constants A and B are calculated from k_n^a values of two reference compounds with known BSO n values and the requirement that for a force constant value of zero the corresponding BSO n value is zero. For the HBs of the AT and GC base pairs investigated in this work, the A and B constants of equation (12) were based upon the references F-H (BSO = 1.0; k^a = 9.432 mDyn Å^{-1}) and [H·F·H]$^-$ (BSO = 0.5; k^a = 0.626 mDyn Å^{-1}) at the ωB97X-D(PCM)/aug-cc-pVTZ level of theory leading to A and B constants valued at 0.564 and 0.256, respectively.

In summary, LMA has advanced over the past years as a powerful bond strength descriptor accounting for both covalent bonds and non-covalent interactions stretching from hydrogen bonds, halogen bonds to tetrel bonds and π-whole interactions. Some recent examples include references [45–47]. Different molecular environments were considered such as systems in solution [48] or in proteins [49]. Another focus has been metal-ligand bonding [50, 51]. The LMA of periodic systems and crystals was recently added to the repertoire [52, 53]. For a comprehensive discussion of LMA theory and its applications the reader is referred to [26] and references therein.

LMA can be complemented with an electron density analysis via Bader's quantum theory of atoms in molecules [54–56]. In particular the covalent character of a chemical bond and/or weak chemical interaction can be assessed via the Cremer–Kraka criterion [57, 58], which is based on the local energy density $H(\mathbf{r})$:

$$H(\mathbf{r}) = G(\mathbf{r}) + V(\mathbf{r}) \tag{13}$$

where $G(\mathbf{r})$ is kinetic energy density (positive, destabilizing) and $V(\mathbf{r})$ is potential energy density (negative, stabilizing).

If the energy density $H(\mathbf{r}_b)$ taken at the bond critical point $\mathbf{r}_b$ of the electron density $\rho(\mathbf{r})$ between the two atoms A and B in question is smaller than zero, the interaction is of covalent character, if it is larger than zero, the interaction is of predominantly electrostatic character [57, 58].

3. Computational details

We calculated equilibrium geometries and subsequent normal vibrational frequencies of the methylated nucleobases 9-methyladenine (i.e. A), 9-methylguanine (i.e. G), 1-methylthymine (i.e. T), and 1-methylcytosine (i.e. C) and their corresponding Watson–Crick base pairs (i.e. 9-methyladenine:1-methylthymine (i.e. AT), 9-methylguanine:1-methylcytosine (i.e. GC)) (see figure 1) [6], using the ωB97X-D functional [59] in combination with Dunning's aug-cc-pVTZ basis set [60, 61]. It is

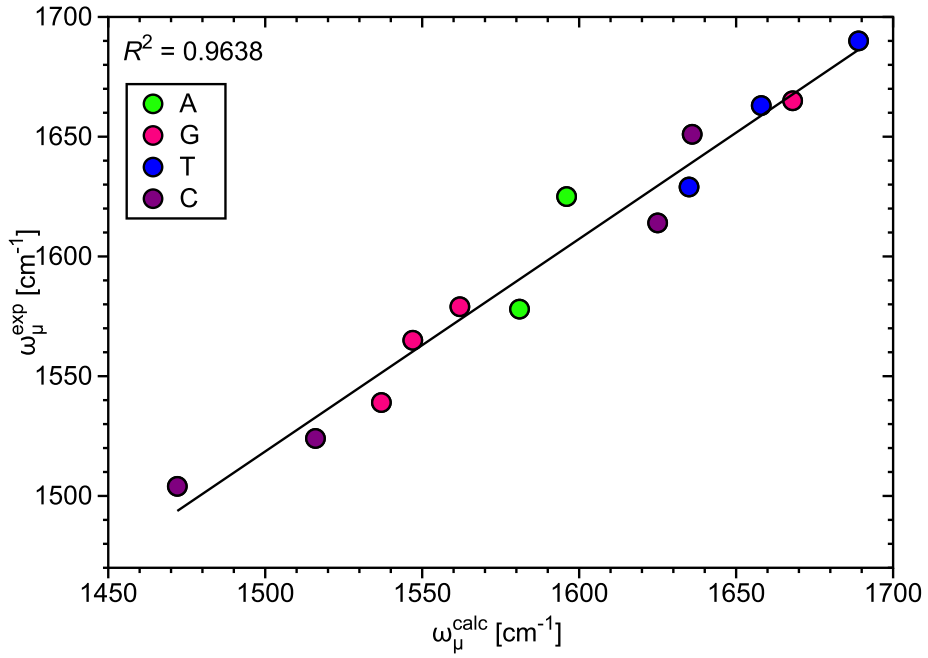

Figure 2. A plot featuring experimental [10] and calculated normal vibrational mode frequencies in cm^{-1}, ω_μ^{exp} and ω_μ^{calc}, respectively, for the deuterated systems A, G, T, and C. The calculated frequencies were computed at the the ωB97X-D(PCM)/aug-cc-pVTZ level of theory in the cavity within the water dielectric medium, as well as scaled for anharmonicity effects by a factor of 0.9614 (see text for details).

noted that all labile amino hydrogen atoms of the nucleobases and base pairs investigated were substituted with deuterium atoms [7] (see figure 1). The polarizable continuum model (PCM)[62] was utilized to create the cavity within the water dielectric medium to simulate hydration effects. Therefore, our model chemistry employs implicit solvation only. Normal vibrational mode frequencies were multiplied by an empirical scaling factor of 0.9614 to correct for anharmonicity effects [63].

Figure 2 which correlates computed normal vibrational mode frequencies (ω_μ^{calc}) for the nucleobases of DNA compared with 2D IR vibrational resonances (ω_μ^{exp}) from measurements of nucleotide monophosphates dissolved in D_2O[10] proves the credibility of choice of model chemistry focusing on probing the sensitive normal vibrational modes of both the isolated nucleobases and their corresponding Watson–Crick base pairs in the fingerprint region (1500−1800 cm^{-1}).

All DFT calculations were carried out with the Gaussian 16 quantum chemistry program [64] using ultra-fine grid integration and tight convergence criterion for the self-consistent field step. LMA was performed with the standalone LModeA package [65]. Second perturbation stabilization energies [$\Delta E^{(2)}$], related to orbital interactions, were calculated using the natural bond orbital (NBO) analysis [66, 67] as implemented in the NBO program [68]. The electron density analysis was performed with the AIMAll program [69].

4. Results and discussion

Table 1 collects bond distances (d), local mode frequencies (ω^a), local mode force constants (k^a), electron densities [$\rho(\mathbf{r}_b)$], energy densities [$H(\mathbf{r}_b)$], and the ratios [$H(\mathbf{r}_b)/\rho(\mathbf{r}_b)$] calculated for the nucleobases and the corresponding Watson–Crick base pairs investigated in this work. In the following sections, the tabulated data is scrutinized.

4.1. Assessment of electronic changes in selected covalent bonds upon base pairing

In figure 3, in the context of the regimes prior to and upon base pairing, differences in distance (Δd) are compared against differences in local mode force constant (Δk^a) for the C=C and C=O covalent bonds which have been suggested to partake in vibrational coupling [10, 18, 19] and the intermolecular hydrogen bonds, in both AT and GC.

Figure 3 reveals that there is a linear relationship between the changes in the distance Δd and changes in the local force constant Δk^a upon base pair formation for both AT and GC base pairs ($R^2 = 0.9585$ and

Table 1. Selected bond distances (d), local mode frequencies (ω^a), local mode force constants (k^a), electron densities [$\rho(\mathbf{r}_b)$], energy densities [$H(\mathbf{r}_b)$], and the ratios [$H(\mathbf{r}_b)/\rho(\mathbf{r}_b)$] for the deuterated nucleobases and base pairs of DNA, calculated at the ωB97X-D(PCM)/aug-cc-pVTZ level of theory in the cavity within the water dielectric medium (see text for details).

system	parameter	d(Å)	k^a (mDyn Å^{-1})	ω^a (cm^{-1})	$\rho(\mathbf{r}_b)$ (e Å^{-3})	$H(\mathbf{r}_b)$ (E$_h$ Å^{-3})	$H(\mathbf{r}_b)/\rho(\mathbf{r}_b)$ (E$_h$/e)
A	C13C6	1.404	6.164	1320	2.145	−2.429	−1.133
	D18N16	1.003	7.449	2680	2.372	−3.820	−1.610
	N14C13	1.340	6.628	1319	2.372	−3.312	−1.396
	N14C12	1.336	6.624	1319	2.332	−3.397	−1.456
	H15C12	1.084	5.541	3180	2.039	−2.332	−1.143
G	C2O1	1.223	10.870	1640	2.783	−4.847	−1.741
	D6N3	1.008	7.275	2648	2.359	−3.791	−1.607
	D14N9	1.004	7.345	2661	2.369	−3.777	−1.595
C	C2O1	1.229	10.467	1610	2.761	−4.790	−1.735
	C9C6	1.348	8.212	1524	2.345	−2.993	−1.276
	D15N8	1.003	7.547	2697	2.374	−3.823	−1.611
	C5N3	1.322	7.375	1392	2.448	−3.554	−1.451
	N3C2	1.356	6.002	1256	2.296	−3.096	−1.349
T	C2O1	1.218	11.266	1670	2.829	−4.955	−1.751
	O9C5	1.221	11.154	1662	2.790	−4.869	−1.745
	C10C7	1.344	8.496	1550	2.361	−3.028	−1.283
	D6N3	1.009	7.286	2650	2.357	−3.818	−1.620
AT	C13C6	1.405	6.197	1324	2.142	−2.421	−1.130
	D20N16	1.017	6.378	2479	2.273	−3.800	−1.672
	N14C13	1.344	6.627	1319	2.342	−3.272	−1.397
	N14C12	1.338	6.685	1325	2.320	−3.392	−1.462
	H15C12	1.084	5.540	3180	2.042	−2.332	−1.142
	C24O23	1.231	10.514	1613	2.728	−4.718	−1.730
	C22O18	1.220	11.077	1656	2.816	−4.923	−1.748
	C27C26	1.345	8.439	1545	2.357	−3.019	−1.281
	N21D17	1.037	4.945	2183	2.164	−3.629	−1.677
	O23D20	1.899	0.176	408	0.195	−0.007	−0.034
	D17N14	1.840	0.259	499	0.275	−0.052	−0.191
	O18H15	2.827	0.052	306	0.032	0.005	0.151
GC	C2O1	1.235	10.174	1587	2.708	−4.662	−1.722
	D8N4	1.033	5.407	2283	2.196	−3.648	−1.661
	D20N14	1.021	6.115	2428	2.240	−3.781	−1.688
	O26C21	1.236	10.117	1583	2.719	−4.687	−1.724
	C24C18	1.347	8.302	1532	2.351	−3.009	−1.280
	N6D3	1.021	6.133	2431	2.252	−3.788	−1.682
	N15C11	1.331	7.139	1369	2.395	−3.441	−1.437
	C21N15	1.350	6.237	1280	2.321	−3.182	−1.371
	D3O1	1.841	0.247	484	0.224	−0.018	−0.078
	N15D8	1.897	0.475	677	0.242	−0.035	−0.146
	O26D20	1.817	0.310	543	0.238	−0.024	−0.101

0.9341, respectively). In both base pairs, the most significant change occurs for the central intermolecular NH donor bond (AT: N21D27, GC: N4D8 respectively) followed by the upper NH donor bond (AT: N16D20, GC: N6D3 respectively). Clearly this reflects that the isolated nucleobases have adjusted mostly in the part forming the middle HB in the base pair.

In order to describe the same changes in bonding via the connection of a potential energy-related property with an electron density-related property, the same differences in local mode force constant (Δk^a) were compared against differences in energy densities [$\Delta H(\mathbf{r}_b)$], which is given by figure 4 for both AT and GC. As shown in figure 4, there is a large scattering, but the main changes in k^a discussed before are accompanied by a decrease in covalent character [$\Delta H(\mathbf{r}_b) > 0$] [57, 58]. Interestingly, C22O18 (AT) and D20N14 (GC) exhibit a slight increase in covalent character. Again, the C=C bonds remain unchanged upon base pairing. Based on these results we conclude that the interaction between C=C and C=O bonds obviously does not cause any substantial change in C=C bond lengths nor in potential energy- and electron density-related properties upon base pairing. In the following, we will focus on the decomposition of the

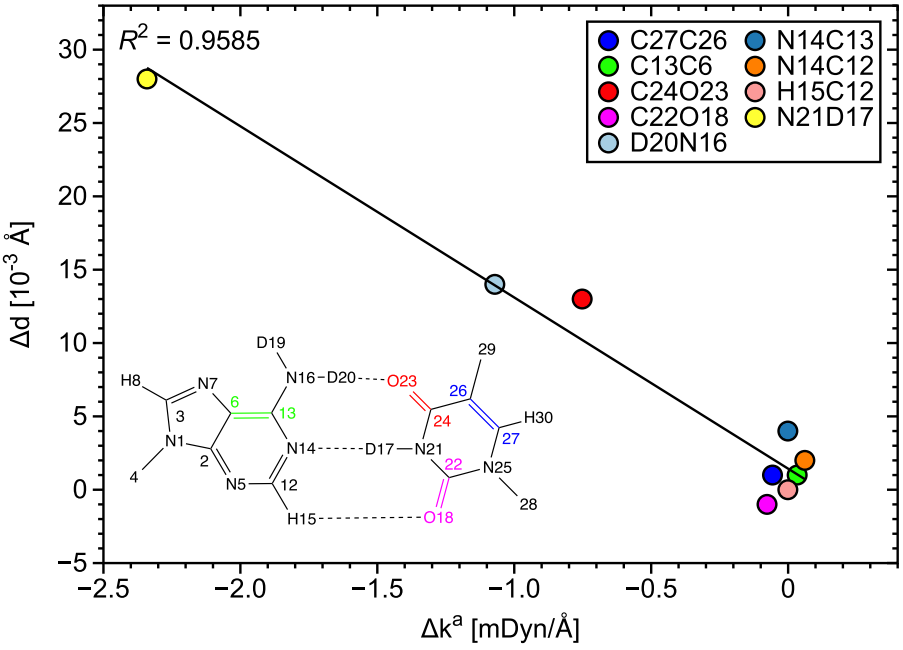

(a)

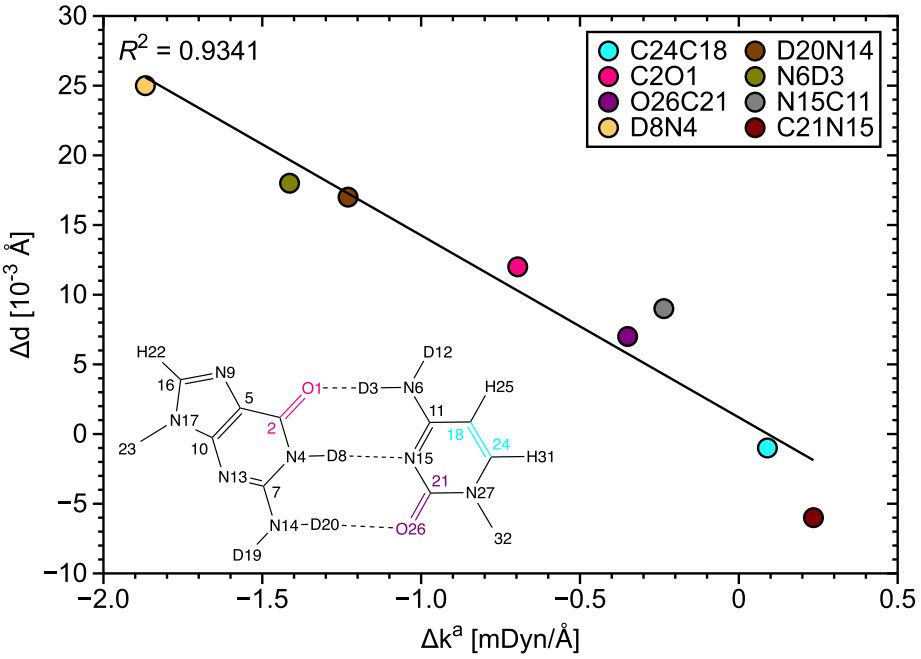

(b)

Figure 3. Selected differences in distance (Δd) versus differences in local mode force constant (Δk^a) for (a) AT and (b) GC. Calculations at the ωB97X-D(PCM)/aug-cc-pVTZ level of theory in the cavity within the water dielectric medium. C=C and C=O bonds suggested to participate in base pair coupling [10, 18, 19] are colored. (see text for details).

characteristic normal vibrational modes via the CNM procedure, followed by the detailed analysis of the HBs involved.

4.2. CNMs

The following discussion is devoted to the consideration of the CNM analysis shown in figures 5–7, which collect the CNM plots of A, G, C, T, AT, and GC, respectively. Our results cover all normal vibrational modes within the in-plane base vibration frequency range of the nucleobases and base pairs. The active IR normal

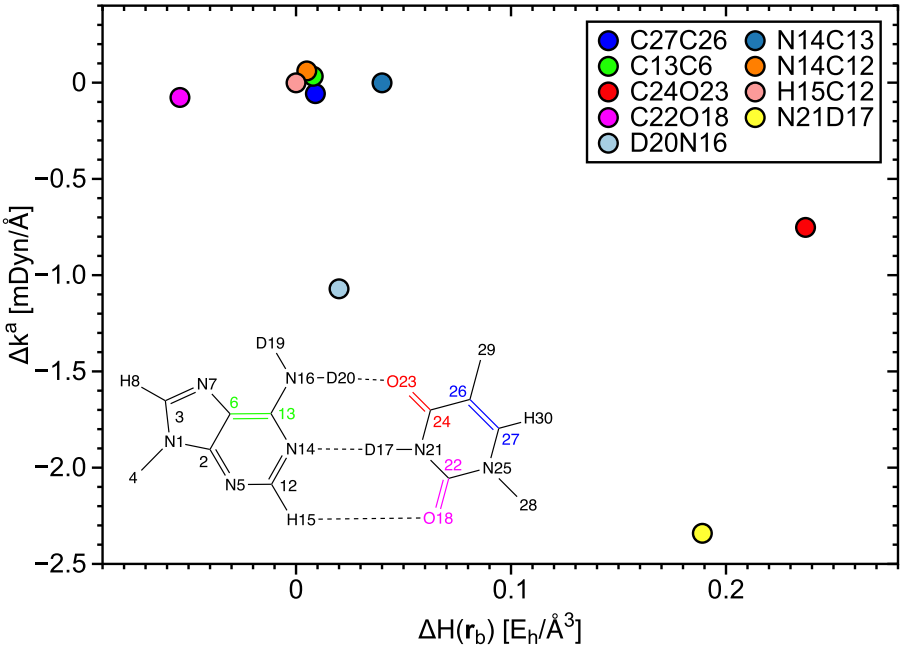

(a)

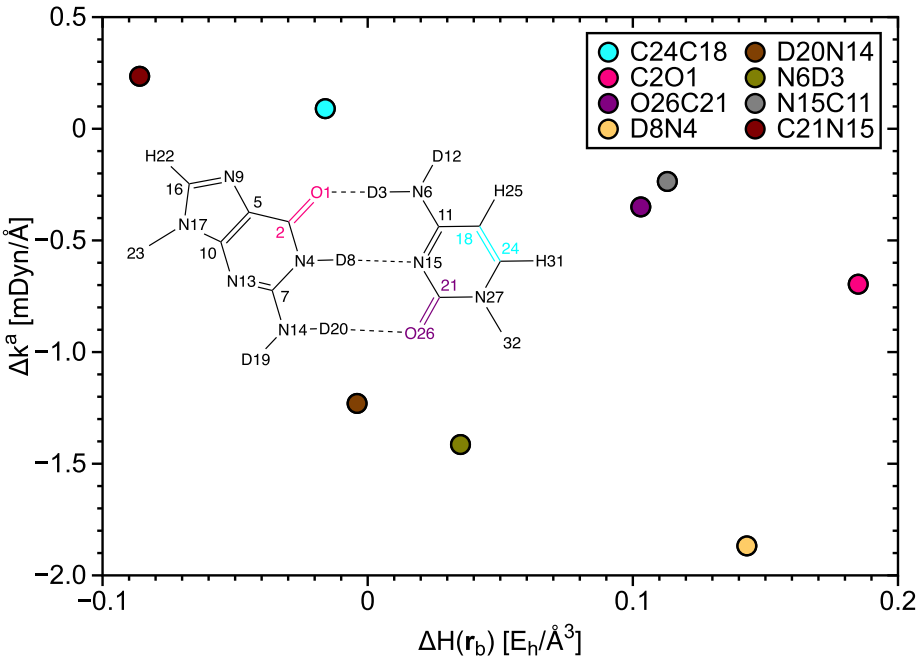

(b)

Figure 4. Selected differences in local mode force constant (Δk^a) versus differences in energy densities [$\Delta H(\mathbf{r}_b)$] for (a) AT and (b) GC. Calculations at the ωB97X-D(PCM)/aug-cc-pVTZ level of theory in the cavity within the water dielectric medium. C=C and C=O bonds suggested to participate in base pair coupling [10, 18, 19] are colored. (see text for details).

vibrational modes of the nucleobases are in agreement with the experimental data [10]. Local mode parameters are denoted by chemical symbols followed by the index number of the atoms according to the specification given in figure 1. Two, three or four symbol strings mean, respectively, bond stretching, bond angle, and dihedral angle local mode parameter. The colors used for the local mode parameters have been kept the same in the CNM plots (sketch and bars) of both the isolated nucleobases and their corresponding base pairs. Whenever referring to the experimental peak assignments, we followed the abbreviation adopted by [10].

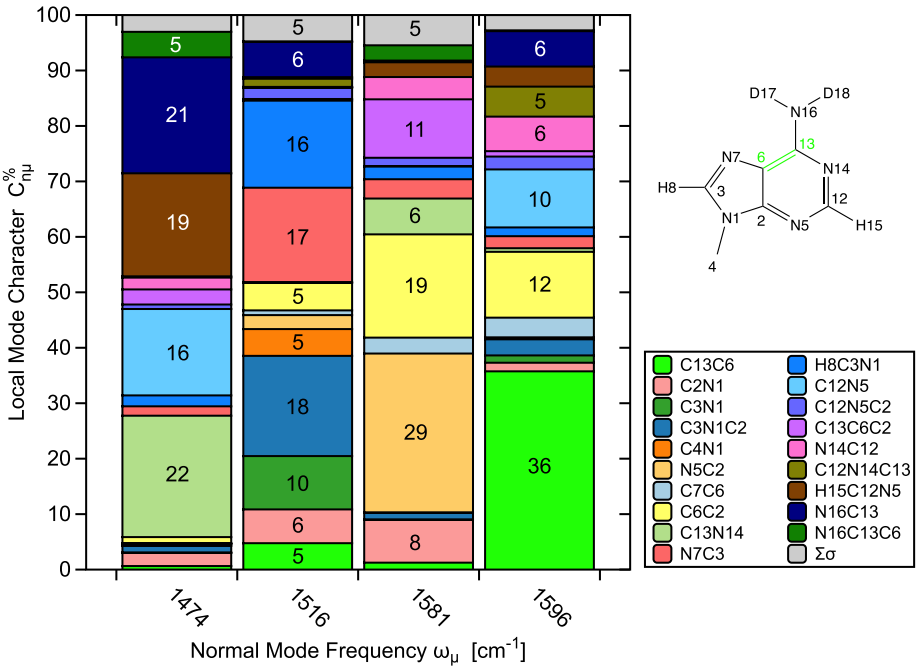

(a)

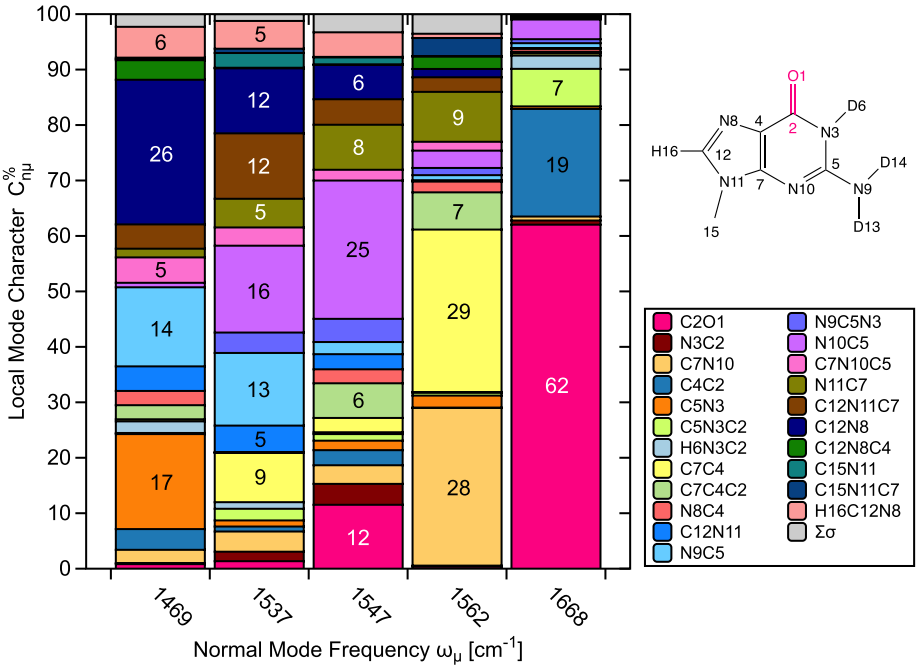

(b)

Figure 5. CNM plot of the characteristic vibrational region of (a) deuterated 9-methyladenine (A) and (b) deuterated 9-methylguanine (G) at the ωB97X-D(PCM)/aug-cc-pVTZ level of theory in the cavity within the water dielectric medium. Normal vibrational mode frequencies are scaled for anharmonicity effects by a factor of 0.9614. $\Sigma\sigma$ comprises the summation of all of the σ local mode contributions below the threshold of 2%.

4.2.1. Deuterated 9-methyladenine (A)

Figure 5(a) shows that the normal vibrational mode at 1596 cm^{-1} is the most localized one in the fingerprint region of A and consists of local vibrational modes whose contribution comes mainly from the pyrimidine ring, including 36% of C13C6. The subsequent normal vibrational mode at 1581 cm^{-1} has 29% of N5C2 character and exhibits some extension to the imidazole ring (8% of C2N1). This ring deformation nature agrees with the peaks denoted as A1 and A2 by Peng *et al* [10], respectively. However, the suggested ND_2 bending contribution to the normal vibrational mode at 1596 cm^{-1} was not observed [3, 7].

4.2.2. Deuterated 9-methylguanine (G)

Based on figure 5(b), although C2O1 accounts for 62% of the normal vibrational mode at 1668 cm^{-1}, C4C2 and C5N3C2 together make 26% of its composition. Yet, this normal vibrational mode is the most localized one in the fingerprint region of G. Moreover, the CNM procedure confirmed the delocalized interpretation of the normal vibrational modes at 1562, 1547, and 1537 cm^{-1}, which is related to G2, G3, and G4, respectively [10]. The amount of delocalization increases from 1562–1537 cm^{-1}.

4.2.3. Deuterated 1-methylcytosine (C)

Figure 6(a) shows that the normal vibrational mode at 1636 cm^{-1} has a major local mode contribution coming from 40% of C9C6, with a trace of C2O1 contribution. H10C6N4 and C6N4 add up to 26% of it as well. This is in an agreement with C2 [10]. On the other hand, the normal vibrational mode at 1625 cm^{-1} contains 67% of C2O1 character, which agrees with C1 [10]. It also contains some trace of C9C6 character. Deuteration makes the equivalent of C3 vanish, and the normal vibrational modes at 1516 and 1472 cm^{-1} comprise in-plane ring vibrations similarly to C4 and C5 [10].

4.2.4. Deuterated 1-methylthymine (T)

Figure 6(b) reveals that the normal vibrational modes at 1689 and 1635 cm^{-1} contain major contributions from C2O1 and O9C5, revealing their interaction. The local mode characters sort of swap their percentage values from one normal vibrational mode to the other. C10C7 accounts for 53% the normal vibrational mode at 1658 cm^{-1}, where minute fractions of C2O1 and O9C5 can be seen as well.

4.2.5. Deuterated 9-methyladenine:1-methylthymine base pair (AT)

Figure 7(a) allows one to quantify the increase in C=O (C24O23 and C22O18) localization of the normal vibrational modes at 1673 and 1609 cm^{-1} in T. Also, there occurs a slight increase in C=C localization of the normal vibrational mode at 1656 cm^{-1}. The normal vibrational modes at 1599 and 1575 cm^{-1} correspond to those active ones (ring deformation) in A. Of particular interest is the normal vibrational mode at 1599 cm^{-1} since our CNM results reveal the interaction between C13C6 in A with the C=O groups in T, mostly C24O23. Such an interaction is also visible in a very small fraction in the normal vibrational modes at 1609 and 1575 cm^{-1}. These important CNM results on the interactions between those groups in AT are in perfect agreement with the literature data [15–17, 19].

4.2.6. Deuterated 9-methylguanine:1-methylcytosine base pair (GC)

Figure 7(b) shows the split of C10O1 character (G) between the normal vibrational modes at 1641 and 1630 cm^{-1}, where interaction with C24C18 from C is verified. On the other hand, C21O16 composes the majority of the normal vibrational mode at 1611 cm^{-1} (C), with a negligible amount of C24C18 contribution. Finally, the normal vibrational modes at 1563, 1544, and 1553 cm^{-1} involve ring deformation in G while that at 1516 cm^{-1} contains contribution from ring deformation in C.

In summary, these results show that the characteristic C=C and C=O bond coupling suggested in the literature [10, 18, 19] can be readily probed via the CNM procedure. The degree of delocalization regarding the fingerprint region can be quantified prior to and upon base pairing. This is an important step forward toward a deeper understanding of how the building blocks of nucleic acids rearrange to form the base pairs, knowledge which could also be useful for the architecture of new so-called unnatural base pairs [70] and modified DNA base pairs with chalcogen bonding [71]. In addition, the same methodology can be employed in the future to explore base stacking effects [6] and might offer a means to probe the optical rotatory response of base complexes [72] based on a more sophisticated model chemistry.

4.3. Hydrogen bond analysis of base pairs

In subsequent we evaluated the HB interactions of the deuterated Watson–Crick base pairs in order to assess how the HB interactions modulate the strength of specific in-plane base vibrations such as C=O and N-D bonds as well as any bonds of corresponding purine (i.e. A and G and) and pyrimidine (i.e. C and T and) rings. Figure 8 shows hydrogen BSOs (n) calculated from local mode force constants (k^a). Hydrogen bond lengths (d) are related with the local mode force constants (k^a), as shown in figure 8. Also, in figure 9, the covalent character of the HB is shown as reflected by $H(\mathbf{r}_b)$ values.

As shown in figure 8, the sensitivity of local mode force constants (k^a) and related BSO n reveals HB2' and HB3 (non-canonical) as the strongest and weakest HBs, respectively, investigated in this work. Interestingly, the strongest hydrogen bond of AT (HB2) is roughly as strong as the weakest hydrogen bond of GC (HB1'). We found the distance of the HBs of the Watson–Crick base pairs investigated to range from

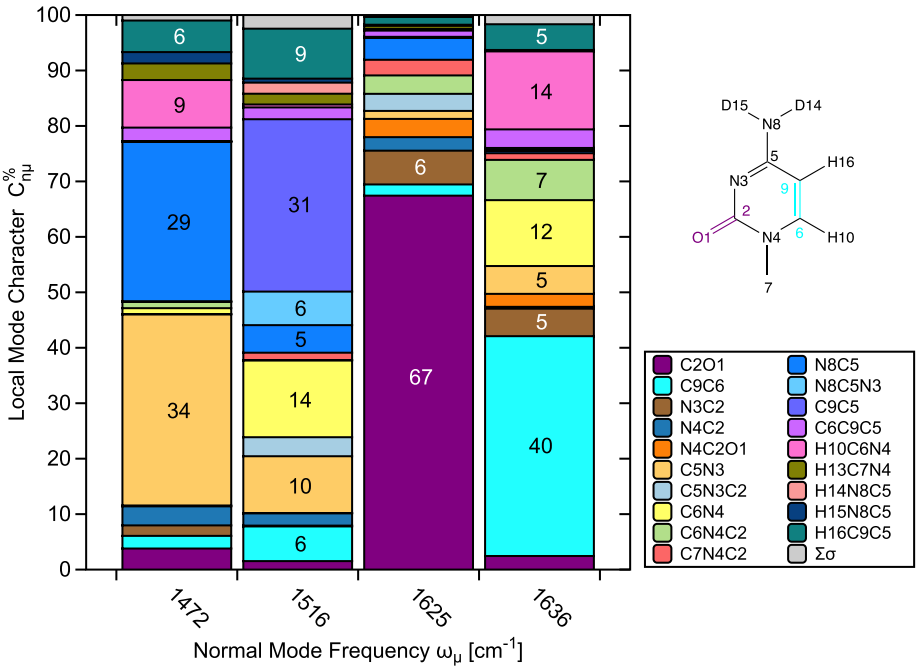

(a)

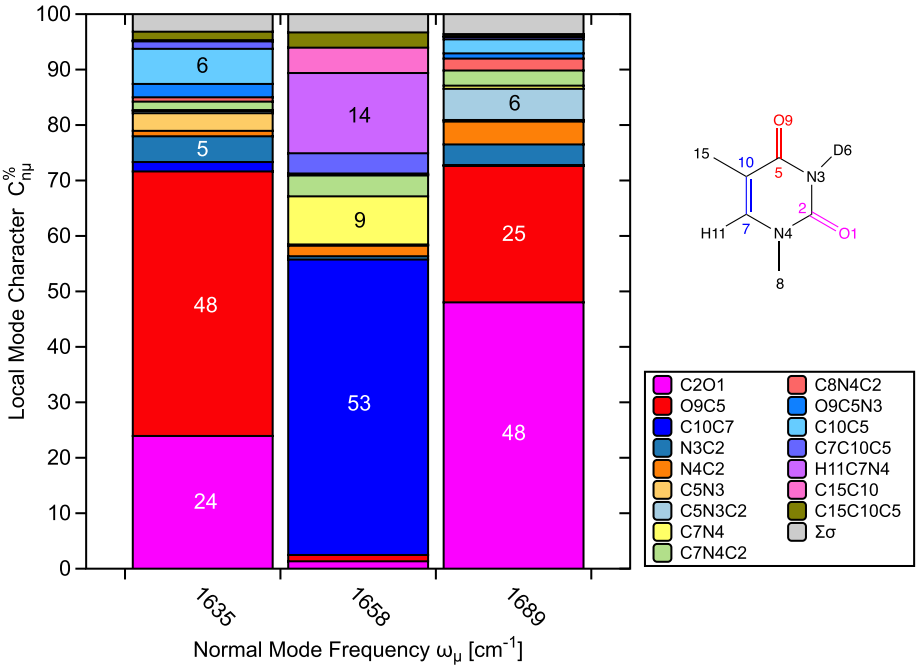

(b)

Figure 6. CNM plot of the characteristic vibrational region of (a) deuterated 1-methylcytosine (C) and (b) deuterated 1-methylthymine (T) at the ωB97X-D(PCM)/aug-cc-pVTZ level of theory in the cavity within the water dielectric medium. Normal vibrational mode frequencies are scaled for anharmonicity effects by a factor of 0.9614. $\Sigma\sigma$ comprises the summation of all of the σ local mode contributions below the threshold of 2%.

1.817 to 2.827 Å (See figure 8). Despite some scattering ($R^2 = 0.8062$), figure 8 shows the generalized Badger rule [43, 44] applies to the hydrogen bonds, i.e. the shortest hydrogen bonds (HB2' and HB3') are also the strongest whereas the longest (HB3) is the weakest. Finally, figure 9 reveals that, according to the Cremer–Kraka criterion [57, 58] for covalent bonding, all hydrogen bonds but the weakest, longest and non-canonical one (HB3) are of covalent character. This is in line with the trend that weaker hydrogen bonds have an increase in electrostatic character, as previously published by our group [73]. It is interesting to note that the corresponding hydrogen bond acceptor (C22O18) of the only electrostatic hydrogen bond (HB3)

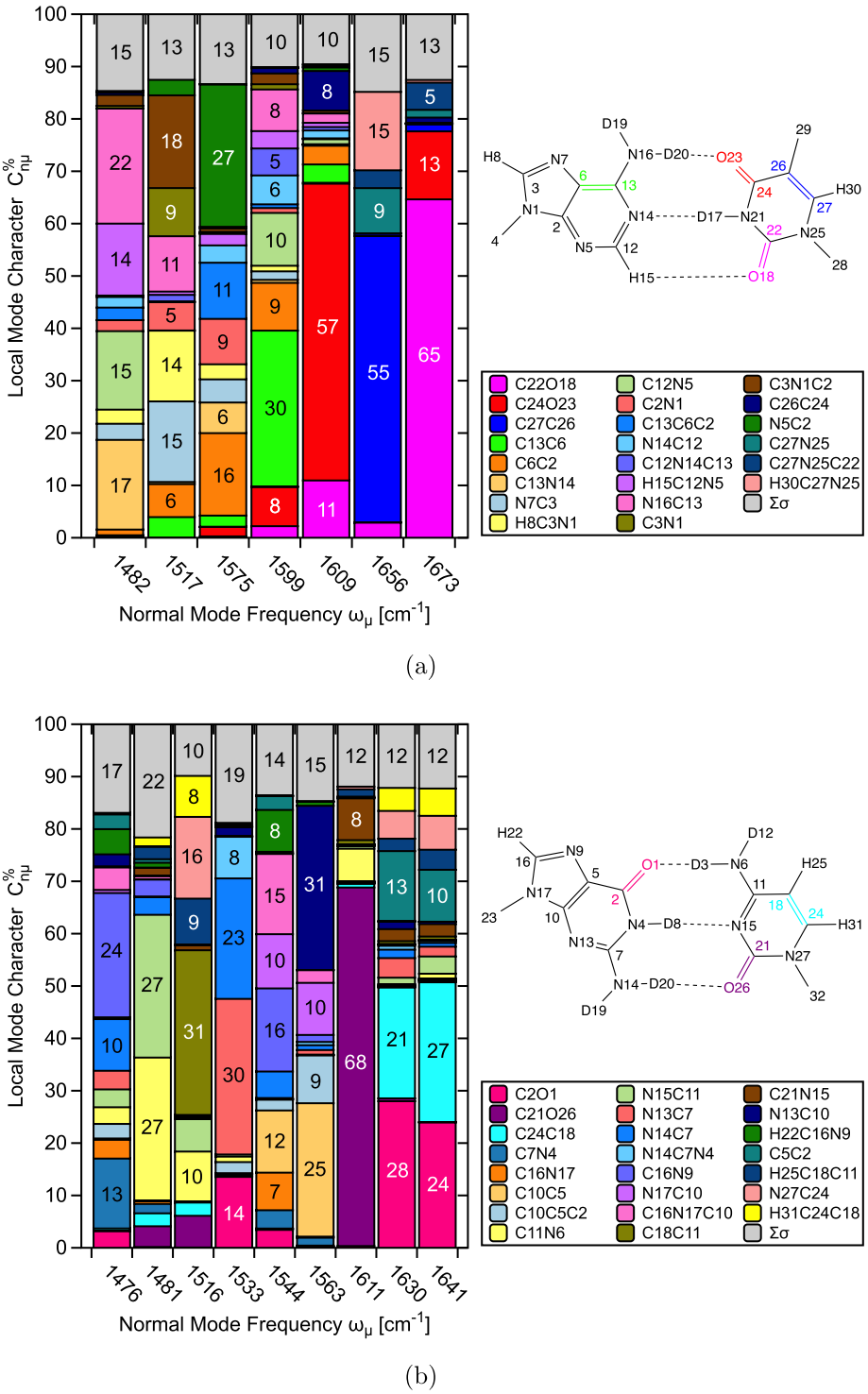

Figure 7. CNM plot of the characteristic vibrational region of (a) deuterated 9-methyladenine:1-methylthymine base pair (AT) and (b) deuterated 9-methylguanine:1-methylcytosine base pair (GC) at the ωB97X-D(PCM)/aug-cc-pVTZ level of theory in the cavity within the water dielectric medium. Normal vibrational mode frequencies are scaled for anharmonicity effects by a factor of 0.9614. $\Sigma\sigma$ comprises the summation of all of the σ local mode contributions below the threshold of 5%.

undergoes a negative change in $H(\mathbf{r}_b)$ upon base pairing, as shown in figure 4. It should be mentioned that for HB3 a bond critical point was detected.

Orbital interaction established between the anti-bonding σ^* orbital of the HB donor molecule and the lone pair (i.e. lp) orbital of the HB acceptor molecule is heavily responsible for HB stabilization [48, 74]. In general, HBs become stronger via the push-pull effects that govern charge transfer events [74]. The extent of charge transfer occurring between the HB acceptor and HB donor molecules can be described in terms of

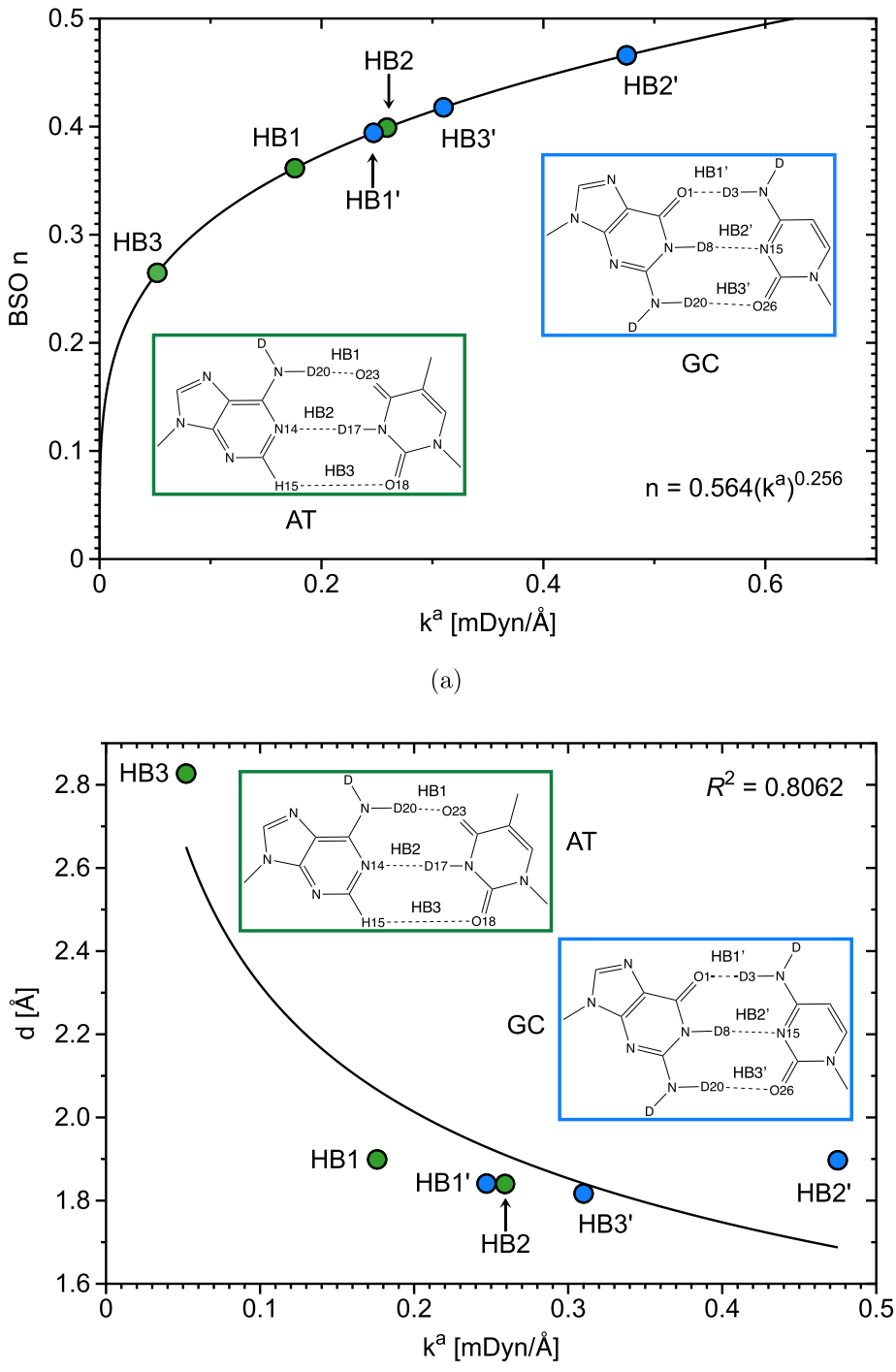

Figure 8. (a) Bond strength order (BSO n) versus local mode force constant (k^a) and (b) bond length (d) versus local mode force constant (k^a) for hydrogen bonds (HBs) of base pairs AT and GC. Calculations at the ωB97X-D(PCM)/aug-cc-pVTZ level of theory in the cavity within the water dielectric medium.

stabilization energy ($\Delta E^{(2)}$) [75]. The $\Delta E^{(2)}$ values of HB1−HB3 of AT reveal that HB2 is stronger in contrast to HB1 and HB3 due to a greater extent of charge transfer [$\Delta E^{(2)}$ = 13.49 (HB1); 21.46 (HB2); 0.39 kcal mol^{-1} (HB3)]. The $\Delta E^{(2)}$ values of HB1'−HB3' of GC reveal that HB2' is stronger than HB1' and HB3' due to a greater extent of charge transfer as well [$\Delta E^{(2)}$ = 18.22 (HB1'); 23.32 (HB2'); 20.20 kcal mol^{-1} (HB3')]. The stabilization energies for the HBs of AT and GC are in line with figure 8(a).

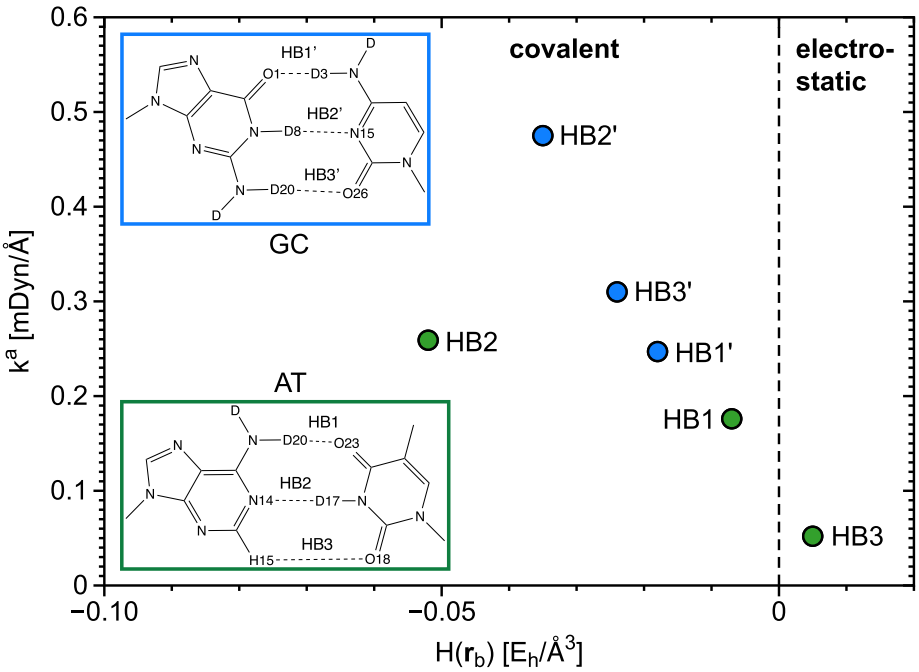

Figure 9. Energy density [$H(\mathbf{r}_b)$] versus local mode force constant (k^a) for hydrogen bonds (HBs) of base pairs AT and GC. Calculations at the ωB97X-D(PCM)/aug-cc-pVTZ level of theory in the cavity within the water dielectric medium.

5. Conclusion

In this work, the degree of delocalization of the fingerprint normal vibrational modes, which is intimately connected to base pair coupling could be quantified and elucidated prior to and upon base pairing. This is a promising approach of detection, herein reported for the first time. We could show that the interaction between C=C and C=O bonds in nucleobases and base pairs of DNA does not cause any substantial change in the C=C bond lengths nor in potential energy-related and electron density-related properties upon base pairing. Instead, such characteristic coupling can be readily probed through the CNM procedure, an integral part of the LMA. In addition, a detailed and quantitative description of the hydrogen bonds involved in the Watson–Crick base pairs was provided. Our findings are expected to have significance to both, the experimental and theoretical vibrational spectroscopy community, and to reach out to the bioengineering community offering an efficient design tool to assess and predict the type and strength of hydrogen bonding in artificial base pairs. The protocol demonstrated within this work can be extended to future works to investigate base stacking or even to gain a better understanding of the optical rotatory response of base complexes, which would involve modified versions of the model chemistry adopted in this work.

Data availability statement

All data that support the findings of this study are included within the article (and any supplementary files).

Acknowledgment

We thank SMU Center for Research Computing for providing generous computational resources. This work was financially supported by the National Science Foundation, Grant CHE 2102461. M Q thanks SMU for the Computational Science and Engineering Fellowship, as well as Bárbara M T C Peluzo for the invaluable help with figure 8(a).

ORCID iDs

Mateus Quintano https://orcid.org/0000-0003-4730-0337
Elfi Kraka https://orcid.org/0000-0002-9658-5626

References

[1] Voet D, Voet J G and Pratt C W 2016 *Fundamentals of Biochemistry: Life at the Molecular Level* 5th edn (New York: Wiley)
[2] Watson J D and Crick F H C 1953 Molecular structure of nucleic acids: a structure for deoxyribose nucleic acid *Nature* **171** 737–8
[3] Banyay M, Sarkar M and Gräslund A 2003 A library of IR bands of nucleic acids in solution *Biophys. Chem.* **104** 477–88
[4] Krummel A T, Mukherjee P and Zanni M T 2003 Inter and intrastrand vibrational coupling in DNA studied with heterodyned 2D-IR spectroscopy *J. Phys. Chem.* B **107** 9165–9
[5] Krummel A T and Zanni M T 2006 DNA vibrational coupling revealed with two-Dimensional infrared spectroscopy: insight into why vibrational spectroscopy is sensitive to DNA structure *J. Phys. Chem.* B **110** 13991–4000
[6] Lee C, Park K-H and Cho M 2006 Vibrational dynamics of DNA. I. vibrational basis modes and couplings *J. Chem. Phys.* **125** 114508–1–114508–16
[7] Lee C and Cho M 2006 Vibrational dynamics of DNA. II. deuterium exchange effects and simulated IR absorption spectra *J. Chem. Phys.* **125** 114509
[8] Lee C, Park K-H, Kim J-A, Hahn S and Cho. M 2006 Vibrational dynamics of DNA. III. molecular dynamics simulations of DNA in water and theoretical calculations of the two-dimensional vibrational spectra *J. Chem. Phys.* **125** 114510
[9] Lee C and Cho M 2007 Vibrational dynamics of DNA: IV. vibrational spectroscopic characteristics of A-, B- and Z-form DNA's *J. Chem. Phys.* **126** 145102
[10] Peng C S, Jones K C and Tokmakoff A 2011 Anharmonic vibrational modes of nucleic acid bases revealed by 2D IR spectroscopy *J. Am. Chem. Soc.* **133** 15650–60
[11] Greve C, Preketes N K, Costard R, Koeppe B, Fidder H, Nibbering E T J, Temps F, Mukamel S and Elsaesser T 2012 N–H stretching modes of adenosine monomer in solution studied by ultrafast nonlinear infrared spectroscopy and *ab initio* calculations *J. Phys. Chem.* A **116** 7636–44
[12] Greve C, Preketes N K, Fidder H, Costard R, Koeppe B, Heisler I A, Mukamel S, Temps F, Nibbering E T J and Elsaesser T 2013 N–H stretching excitations in adenosine-thymidine base pairs in solution: pair geometries, infrared line shapes and ultrafast vibrational dynamics *J. Phys. Chem.* A **117** 594–606
[13] Le Sueur A L, Horness R E and Thielges M C 2015 Applications of two-dimensional infrared spectroscopy *Analyst* **140** 4336–49
[14] Sanstead P J, Stevenson P and Tokmakoff A 2016 Sequence-dependent mechanism of DNA oligonucleotide dehybridization resolved through infrared spectroscopy *J. Am. Chem. Soc.* **138** 11792–801
[15] Hithell G, Shaw D J, Donaldson P M, Greetham G M, Towrie M, Burley G A, Parker A W and Hunt N T 2016 Long-range vibrational dynamics are directed by Watson–Crick base pairing in duplex DNA *J. Phys. Chem.* B **120** 4009–18
[16] Hithell G, González-Jiménez M, Greetham G M, Donaldson P M, Towrie M, Parker A W, Burley G A, Wynne K and Hunt N T 2017 Ultrafast 2D-IR and optical Kerr effect spectroscopy reveal the impact of duplex melting on the structural dynamics of DNA *Phys. Chem. Chem. Phys.* **19** 10333–42
[17] Hithell G, Donaldson P M, Greetham G M, Towrie M, Parker A W, Burley G A and Hunt N T 2018 Effect of oligomer length on vibrational coupling and energy relaxation in double-stranded DNA *Chem. Phys.* **512** 154–64
[18] Jiang Y and Wang L 2019 Development of vibrational frequency maps for nucleobases *J. Phys. Chem.* B **123** 5791–804
[19] Jiang Y and Wang L 2020 Modeling the vibrational couplings of nucleobases *J. Chem. Phys.* **152** 084114
[20] Fick R J, Liu A Y, Nussbaumer F, Kreutz C, Rangadurai A, Xu Y, Sommer R D, Shi H, Scheiner S and Stelling A L 2021 Probing the hydrogen-bonding environment of individual bases in DNA duplexes with isotope-edited infrared spectroscopy *J. Phys. Chem.* B **125** 7613–27
[21] Konkoli Z and Cremer D 1998 A new way of analyzing vibrational spectra. I. derivation of adiabatic internal modes *Int. J. Quantum Chem.* **67** 1–9
[22] Konkoli Z, Larsson J A and Cremer D 1998 A new way of analyzing vibrational spectra. II. comparison of internal mode frequencies *Int. J. Quantum Chem.* **67** 11–27
[23] Konkoli Z and Cremer D 1998 A new way of analyzing vibrational spectra. III. characterization of normal vibrational modes in terms of internal vibrational modes *Int. J. Quantum Chem.* **67** 29–40
[24] Konkoli Z, Larsson J A and Cremer D 1998 A new way of analyzing vibrational spectra. IV. application and testing of adiabatic modes within the concept of the characterization of normal modes *Int. J. Quantum Chem.* **67** 41–55
[25] Cremer D, Larsson J A and Kraka E 1998 New developments in the analysis of vibrational spectra on the use of adiabatic internal vibrational modes *Theor. Comput. Chem* ed C Parkanyi (Amsterdam: Elsevier) pp 259–327
[26] Kraka E, Zou W and Tao Y 2020 Decoding chemical information from vibrational spectroscopy data: local vibrational mode theory *WIREs: Comput. Mol. Sci.* **10** 1480
[27] Wilson E B, Decius J C and Cross P C 1955 *Molecular Vibrations: the Theory of Infrared and Raman Vibrational Spectra* (New York: McGraw-Hill)
[28] Woodward L A 1972 *Introduction to the Theory of Molecular Vibrations and Vibrational Spectroscopy* (Oxford: Oxford University Press)
[29] Herzberg G 1945 *Molecular Spectra and Molecular Structure, II. Infrared and Raman Spectra of Polyatomic Molecules* (New York: Van Nostrand)
[30] Herzberg G and Huber K P 1979 *Molecular Spectra and Molecular Structure. IV. Constants of Diatomic Molecules* (New York: Van Nostrand, Reinhold)
[31] Califano S 1976 *Vibrational States* (London: Wiley)
[32] Zou W, Izotov D and Cremer D 2011 New way of describing static and dynamic deformations of the Jahn-Teller type in ring molecules *J. Phys. Chem.* A **115** 8731–42
[33] Zou W, Filatov M and Cremer D 2012 Bond pseudorotation, Jahn-Teller and Pseudo-Jahn-teller effects in the cyclopentadienyl cation and its pentahalogeno derivatives *Int. J. Quantum Chem.* **112** 3277–88
[34] Zou W and Cremer D 2014 Description of bond pseudorotation, bond pseudolibration and ring pseudoinversion processes caused by the Pseudo-Jahn-Teller effect: fluoro derivatives of the cyclopropane radical cation *Aust. J. Chem.* **67** 435
[35] Cremer D and Pople J A 1975 General Definition of ring puckering coordinates *J. Am. Chem. Soc.* **97** 1354–8
[36] Barone V, Alessandrini S, Biczysko M, Cheeseman J R, Clary D C, McCoy A B, DiRisio R J, Neese F, Melosso M and Puzzarini C 2021 Computational molecular spectroscopy *Nat. Rev. Methods Primers* **1** 1–27
[37] Baiz C R *et al* 2020 Vibrational spectroscopic map, vibrational spectroscopy and intermolecular interaction *Chem. Rev.* **120** 7152–218

[38] Beć K B, Grabska J and Huck C W 2021 Current and future research directions in computer-aided near-infrared spectroscopy: a perspective *Spectrochim. Acta A* **254** 1–11
[39] Wilson E B 1941 Some mathematical methods for the study of molecular vibrations *J. Chem. Phys.* **9** 76–84
[40] Quintano M and Kraka E 2022 Theoretical insights into the linear relationship between pK_a values and vibrational frequencies *Chem. Phys. Lett.* **803** 139746
[41] Verma N, Tao Y, Zou W, Chen X, Chen X, Freindorf M and Kraka E 2020 A critical evaluation of vibrational Stark effect (VSE) probes with the local vibrational mode theory *Sensors* **20** 2358
[42] Zou W and Cremer D 2016 C_2 in a box: determining its intrinsic Bond Strength for the $X^1\Sigma_g^+$ ground state *Chem. Eur. J.* **22** 4087–97
[43] Cremer D and Kraka E 2010 From molecular vibrations to bonding, chemical reactions and reaction mechanism *Curr. Org. Chem.* **14** 1524–60
[44] Kraka E, Larsson J A and Cremer D 2010 Generalization of the Badger Rule based on the use of adiabatic vibrational modes *Computational Spectroscopy* ed J Grunenberg (New York: Wiley) pp 105–49
[45] Delgado A A A, Humason A, Kalescky R, Freindorf M and Kraka E 2021 Exceptionally long covalent CC bonds - a local vibrational mode study *Molecules* **26** 950
[46] Yannacone S, Freindorf M, Tao Y, Zou W and Kraka E 2020 Local vibrational mode analysis of π-Hole interactions between aryl donors and small molecule acceptors *Crystals* **10** 556
[47] Oliveira V P, Marcial B L, Machado F B and Kraka E 2021 relating bond strength and nature to the thermodynamic stability of hypervalent togni-type iodine compounds *ChemPlusChem* **86** 1199–1210
[48] Delgado A A A, Sethio D, Munar I, Aviyente V and Kraka E 2020 Local vibrational mode analysis of ion–solvent and solvent–solvent interactions for hydrated Ca^{2+} clusters *J. Chem. Phys.* **153** 224303
[49] Freindorf M and Kraka E 2020 critical assessment of the FeC and CO bond strength in carboxymyoglobin - a qm/mm local vibrational mode study *J. Mol. Model.* **26** 281
[50] Kraka E and Freindorf M 2020 Characterizing the metal ligand bond strength via vibrational spectroscopy: the metal ligand electronic parameter (MLEP) *Topics in Organometallic Chemistry- New Directions in the Modeling of Organometallic Reactions* vol 67, ed Ai Lledós and G Ujaque (Berlin: Springer) pp 1–43
[51] McCutcheon M, Freindorf M and Kraka E 2022 Bonding in nitrile photo-dissociating ruthenium drug candidates – a local vibrational mode study *J. Chem. Phys.* **157** 014301–1–014301–15
[52] Tao Y, Zou W, Sethio D, Verma N, Qiu Y, Tian C, Cremer D and Kraka E 2019 In situ measure of intrinsic bond strength in crystalline structures: local vibrational mode theory for periodic systems *J. Chem. Theory Comput.* **15** 1761–76
[53] Nanayakkara S, Tao Y and Kraka E 2022 Capturing Individual Hydrogen Bond Strengths in Ices via Periodic Local Vibrational Mode Theory: Beyond the Lattice Energy Picture *J. Chem. Theory Comput.* **18** 562–79
[54] Bader R F W 1990 *Atoms in molecules: a quantum theory International Series Of Monographs on Chemistry* (New York: Oxford University Press)
[55] Bader R F W 1998 Atoms in molecules *Chem. Rev.* **1** 64
[56] Popelier P L 2000 *Atoms in Molecules: An Introduction* (Hoboken, NJ: Prentice Hall)
[57] Cremer D and Kraka E 1984 Chemical bonds without bonding electron density? does the difference electron-density analysis suffice for a description of the chemical bond? *Angew. Chem., Int. Ed.* **23** 627–8
[58] Cremer D and Kraka E 1984 A description of the chemical bond in terms of local properties of electron density and energy *Croatica Chem. Acta* **57** 1259–81
[59] Chai J-D and Head-Gordon M 2008 Long-range corrected hybrid density functionals with damped atom–atom dispersion corrections *Phys. Chem. Chem. Phys.* **10** 6615–20
[60] Dunning T H 1989 Gaussian basis sets for use in correlated molecular calculations. I. The atoms boron through neon and hydrogen *J. Chem. Phys.* **90** 1007–23
[61] Kendall R A, Dunning T H and Harrison R J 1992 Electron affinities of the first-row atoms revisited. systematic basis sets and wave functions *J. Chem. Phys.* **96** 6796–806
[62] Tomasi J, Mennucci B and Cammi R 2005 Quantum Mechanical continuum solvation models *Chem. Rev.* **105** 2999–3094
[63] Scott A P and Radom L 1996 Harmonic Vibrational frequencies: an evaluation of Hartree-Fock, Møller-Plesset, quadratic configuration interaction, density functional theory and semiempirical scale factors *J. Phys. Chem.* **100** 16502–13
[64] Frisch M J, Trucks G W, Schlegel H B, Scuseria G E, Robb M A, Cheeseman J R, Scalmani G, Barone V, Petersson G A, Nakatsuji H Gaussian 16 Revision C.01, 2016. Gaussian Inc. Wallingford CT
[65] Zou W, Tao Y, Freindorf M, Makoś M Z, Verma N, Cremer D and Kraka E 2021 Local vibrational mode analysis (LModeA) *Computational and Theoretical Chemistry Group (Catco)* (Dallas, TX: Southern Methodist University)
[66] Weinhold F, Landis C R and Glendening E D 2016 What is NBO analysis and how is it useful? *Int. Rev. Phys. Chem.* **35** 399–440
[67] Weinhold F and Landis C R 2001 Natural bond orbital and extensions of localized bonding concepts *Chem. Educ. Res. Pract.* **2** 91–104
[68] Weinhold F and Landis C R 2003 *Valency and Bonding: A Natural Bond Orbital Donor-Acceptor Perspective* (Cambridge, Madison: Cambridge University Press, Theoretical Chemistry Institute, University of Wisconsin)
[69] Keith T A 2017 AIMAll Version 17. 11.14 K Gristmill Software Kansas (aim.tkgri stmill.com)
[70] Beiranvand N, Freindorf M and Kraka E 2021 Hydrogen bonding in natural and unnatural base pairs - explored with vibrational spectroscopy *Molecules* **26** 2268–1–2268–22
[71] Sharma K D, Kathuria P, Wetmore S D and Sharma P 2020 Can modified DNA base pairs with chalcogen bonding expand the genetic alphabet? a combined quantum chemical and molecular dynamics simulation study *Phys. Chem. Chem. Phys.* **22** 23754–65
[72] Goldsmith M-R, Jayasuriya N, Beratan D N and Wipf P 2003 Optical rotation of noncovalent aggregates *J. Am. Chem. Soc.* **125** 15696–7
[73] Freindorf M, Kraka E and Cremer D 2012 A comprehensive analysis of hydrogen bond interactions based on local vibrational modes *Int. J. Quantum Chem.* **112** 3174–87
[74] Tao Y, Zou W and Kraka E 2017 Strengthening of hydrogen bonding with the push-pull effect *Chem. Phys. Lett.* **685** 251–8
[75] Reed A E, Curtiss L A and Weinhold F 1988 Intermolecular interactions from a natural bond orbital, donor-acceptor viewpoint *Chem. Rev.* **88** 899–926